# A LEED STUDY OF ETHANE FILMS ADSORBED ON GRAPHITE IN THE MONOLAYER RANGE

J. SUZANNE, J.L. SEGUIN, H. TAUB * and J.P. BIBERIAN

*Faculté des Sciences de Luminy, Département de Physique, Case 901, F-13288 Marseille Cédex, France*

Ethane monolayers adsorbed on graphite in the monolayer range have been studied by high-resolution LEED in the range $40 < T < 85$ K. Three two-dimensional solid phases $S_1$, $S_2$, $S_3$ have been observed at temperatures below 60 K in agreement with previous neutron diffraction experiments. The LEED studies show that $S_1$ is a $4 \times \sqrt{3}$ commensurate rectangular centred cell with a herring-bone packing. It transforms at 64 K into a short range ordered solid $I_1$ having the hexagonal symmetry of a $2 \times 2$ commensurate phase. Then $I_1$ transforms continuously into an isotropic liquid-like phase with increasing temperature. $S_2$ appears to be a $10 \times 2\sqrt{3}$ rectangular structure with 12 molecules per unit cell. Finally $S_3$ has a commensurate $\sqrt{3} \times \sqrt{3}$ unit cell with molecules probably standing on their methyl tripods. This is the first physisorbed system where a complete solution of an orientationally ordered structure ($S_1$) has been obtained by combining neutron diffraction and LEED experiments.

## 1. Introduction

It is now well known that physically adsorbed monolayers on crystal surfaces provide experimental models of two-dimensional (2D) matter [1–7]. Such is the case for rare gases, nitrogen, hydrogen or oxygen adsorbed on graphite [1–4] or rare gases adsorbed on metal surfaces [5–7]. Among the various adsorbates, non-spherical molecules, having a rod-like symmetry, give rise to new kinds of phenomena: 2D polymorphism [8,9] and orientational ordering [10–12] are some of the features presented by these adsorbate species. One of the most extensively studied systems has been nitrogen on graphite. This system has been investigated by numerous techniques [10,11,13–15] and it shows commensurate and incommensurate 2D solid phases, 2D melting and 2D orientational ordering [10,11]. LEED experiments have given valuable crystallographic information. They have shown that the orientationally ordered

---

* Permanent address: Department of Physics, University of Missouri–Columbia, Columbia, Missouri 65211, USA.

phase of $N_2$ molecules physisorbed on graphite is a two-sublattice herring-bone structure [11].

Neutron diffraction experiments have been performed on a slightly more complicated non-spherical molecule adsorbed on graphite, namely ethane [16–21]. This system displays a very complicated and interesting phase diagram [18,20]. A large number of Bragg peaks have been observed, and profile analysis of the neutron spectra [12,18,20] has been used to determine the structure of 2D solids. Three solid phases, $S_1$, $S_2$ and $S_3$, have been discovered. They appear successively with increasing coverage at low temperature. The melting of $S_1$ and $S_2$ occurs via intermediate phases $I_1$ and $I_2$ in a first order melting transition. Then $I_1$ and $I_2$ transform continuously into a fluid-like phase.

The problem of uniqueness of the structure determined by neutron diffraction has been addressed. In a previous paper [21], we proposed two possible unit cells for solid $S_1$, one of them being a herring-bone structure with a rectangular commensurate $4 \times \sqrt{3}$ unit cell. Furthermore, two hypotheses have been suggested for $I_1$: an orientationally disordered hexagonal structure or a chain-like structure.

Some of the results put the ethane–graphite system in close analogy with nitrogen. In addition, they raise questions which are of current interest concerning the herring-bone order and the melting of such a structure [22–24]. For instance, it has been shown that the transition from long range herring-bone order (smectic E) to short range positional but true bond-orientational order (smectic B) is first order in the 650BC liquid crystal [23,24], whereas the transition from smectic B to smectic A with isotropic intralayer correlations is continuous. Such a result is quite analogous to the sequence $S_1 \rightarrow I_1 \rightarrow$ isotropic fluid observed in ethane adsorbed on graphite. Hence, a better understanding of the ethane–graphite system could contribute to the controversial discussion about the nature of 2D melting [25–30].

The paper will present recent high resolution LEED experiments which provide three important results: the $S_1$ structure, the $S_2$ unit cell and the nature of the intermediate phase $I_1$.

## 2. Summary of the neutron diffraction experiments

The experiments have been described elsewhere [16–21]. Let us recall that they have been performed at the University of Missouri Research Reactor Facility (MURR) and at the Institut Laue–Langevin (ILL) in Grenoble. The substrates used were Grafoil (MURR) and Papyex (ILL). The deuterated form of ethane was used to enhance the coherent neutron cross section of the film.

The results given in refs. [16–21] are best summarized in the very schematic and tentative phase diagram presented in fig. 1. It shows the three solid phases

$S_1$, $S_2$ and $S_3$, plus two intermediate phases $I_1$ and $I_2$, plus a liquid-like phase L. It is important to notice that the solid–solid transitions and the solid–intermediate phase transitions are first order as evidenced by phase coexistence.
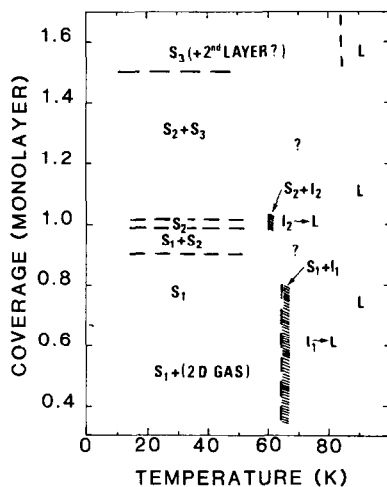


Fig. 1. Schematic and tentative phase diagram for ethane adsorbed on graphite from refs. [18–20]. One sees the domain of existence of the three solid phases $S_1$, $S_2$ and $S_3$, the intermediate phase $I_1$ and $I_2$ and the liquid-like phase L. Phase coexistences, signature of first order phase transitions, are indicated. The $I_1 \rightarrow L$ and $I_2 \rightarrow L$ transitions are continuous.

Coverage one is defined as the coverage corresponding to the knee of an adsorption isotherm [18–20]; it leads to an areal density of $\simeq 17.5$ Å$^2$ per molecule.

## 2.1. Solid $S_1$ (coverage $\leq 0.8$ monolayer)

Two different unit cells have been proposed for the low coverage solid $S_1$, called $S_1(A)$ and $S_1(B)$ [18,20]. Figs. 2 and 3 present the two structures. To determine the molecular orientations, profile lineshape analysis of the neutron diffraction patterns has been done. The calculations are based on the modified Warren theory of diffraction for 2D polycrystals in the form appropriate to neutron scattering [12]. Each of the two structures gives reasonable agreement with the observed peak intensities. $S_1(A)$ has an oblique cell with one molecule. It is partially registered along the *a* direction where the distance between molecules is twice the lattice constant of graphite within experimental errors. $S_1(B)$ is a $4 \times \sqrt{3}$ rectangular commensurate structure with two molecules per unit cell. It has a herring-bone-like packing. The different arguments to
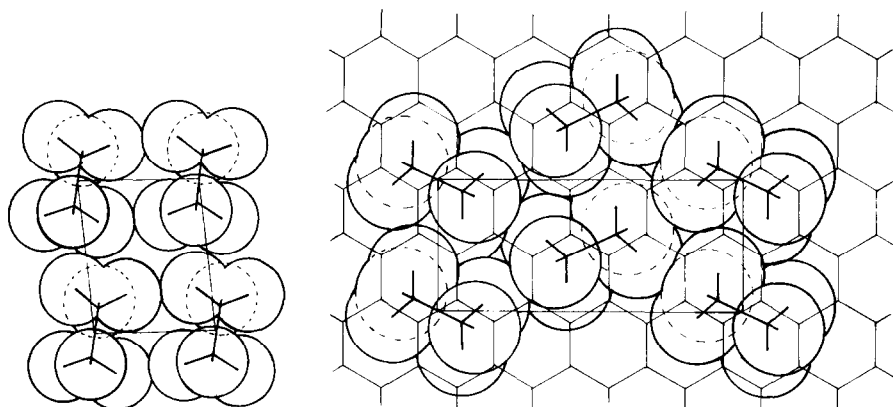
Fig. 2. Structure of the $S_1(A)$ phase [16–20]. The unit cell is oblique with $|a| = 4.95$ Å, $|b| = 3.94$ Å and $(a, b) \simeq 85°$.

Fig. 3. Structure of the $S_1(B)$ phase from refs. [18–20]. The unit cell is $4 \times \sqrt{3}$ commensurate rectangular centred with a herring-bone packing. The angle between the C–C axes and the $a$ basis vector is $+23°$ or $-23°$ for the centre molecules or corner molecules, respectively. This implies glide plane symmetries and the structure belongs to the p2gg group.

discriminate between the two alternative models are discussed in refs. [18,20]. Indeed, model B is in many ways similar to the nitrogen herring-bone structure. The fact that the angle between the C–C axis of each molecule in the unit cell and the $a$ direction are equal (23°), but with opposite signs, implies the existence of two glide planes along the [10] and [01] directions. The unit cell belongs to the 2D group symmetry p2gg [31]. It should be noticed that in the case of model B, unlike nitrogen, the distance between the corner molecules is different from that between a corner and centre molecule.

The $S_1$ structure is stable from 10 to 64 K. At $T \simeq 64$ K, $S_1$ transforms into a new phase $I_1$. Neutron diffraction shows only one peak which is broader than the $S_1$ peaks, but still narrower than one should expect for a liquid. The coherence length of $S_1$ is 120 Å, whereas that of $I_1$ is 50 Å. The single diffraction peak can be indexed as that of a commensurate $2 \times 2$ structure. It corresponds to a distance between molecules equal to 4.92 Å. Two possibilities have been considered to explain this intermediate phase [16,18–20]:

(a) $I_1$ is an orientationally disordered structure and the transition is similar to that of nitrogen except that in the case of ethane it is clearly first order as proved by coexistence of $S_1$ and $I_1$.

(b) $I_1$ could be a 2D liquid-crystal-like smectic phase where molecules lie in parallel rows which are equidistant but with the centre of mass of the molecules randomly positioned within a row.

Increasing the temperature above the $S_1 \to I_1$ phase transition results in a gradual broadening of the Bragg peak whose coherence length reaches 25 Å when $T \simeq 89$ K. Hence, to within the experimental resolution, $I_1$ tranforms continuously into an isotropic liquid-like phase.

Let us notice that $I_1$ has the same areal density as $S_1(B)$ and a 8% lower density than $S_1(A)$.

## 2.2. Solid $S_2$ (coverage $\simeq 1$ monolayer)

The unit cell proposed for $S_2$ [17–21] is represented in fig. 4. It is an oblique cell with two molecules. The experimental diffraction pattern agrees reasonably well with the profile analysis fit obtained for the first six peaks.

Like $S_1$, $S_2$ transforms into an intermediate phase $I_2$ at $T \simeq 60$ K through a coexistence region, the signature of a first order transition. This new intermediate phase shows again only one Bragg peak at $Q \simeq 1.51$ Å$^{-1}$ corresponding to a distance between molecules equal to 4.79 Å. This phase might be an incommensurate hexagonal structure corresponding to a compression of the $2 \times 2$ $I_1$ phase [18,20]. The coherence length of $S_2$ is 120 Å like $S_1$, whereas that of $I_2$ is 35 Å, smaller than that of $I_1$. Hence, there is close analogy between the melting of $S_1$ and that of $S_2$.
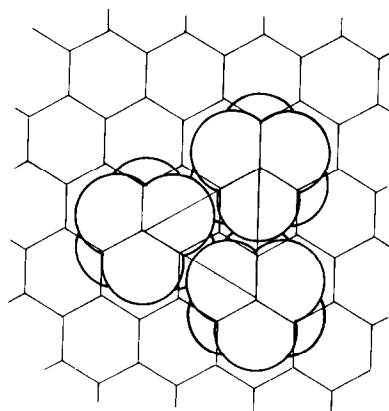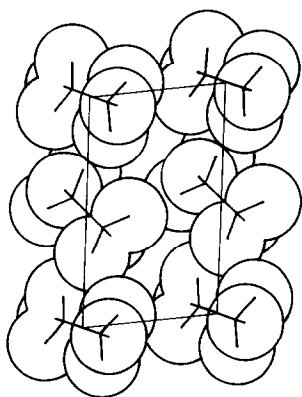


Fig. 4. Structure of the $S_2$ phase [17–20]. The unit cell is oblique with $|a| = 4.35$ Å, $|b| = 7.50$ Å and $(a, b) = 81.5°$. There are two molecules per unit cell.

Fig. 5. Structure of the $S_3$ phase [17–20]. It is a commensurate $\sqrt{3} \times \sqrt{3}$ phase with molecules probably orientated with the C–C bond perpendicular to the graphite surface. The relative position above the surface is not known and the representation in the picture is just to indicate one possibility. The distance between the molecules is 4.26 Å.
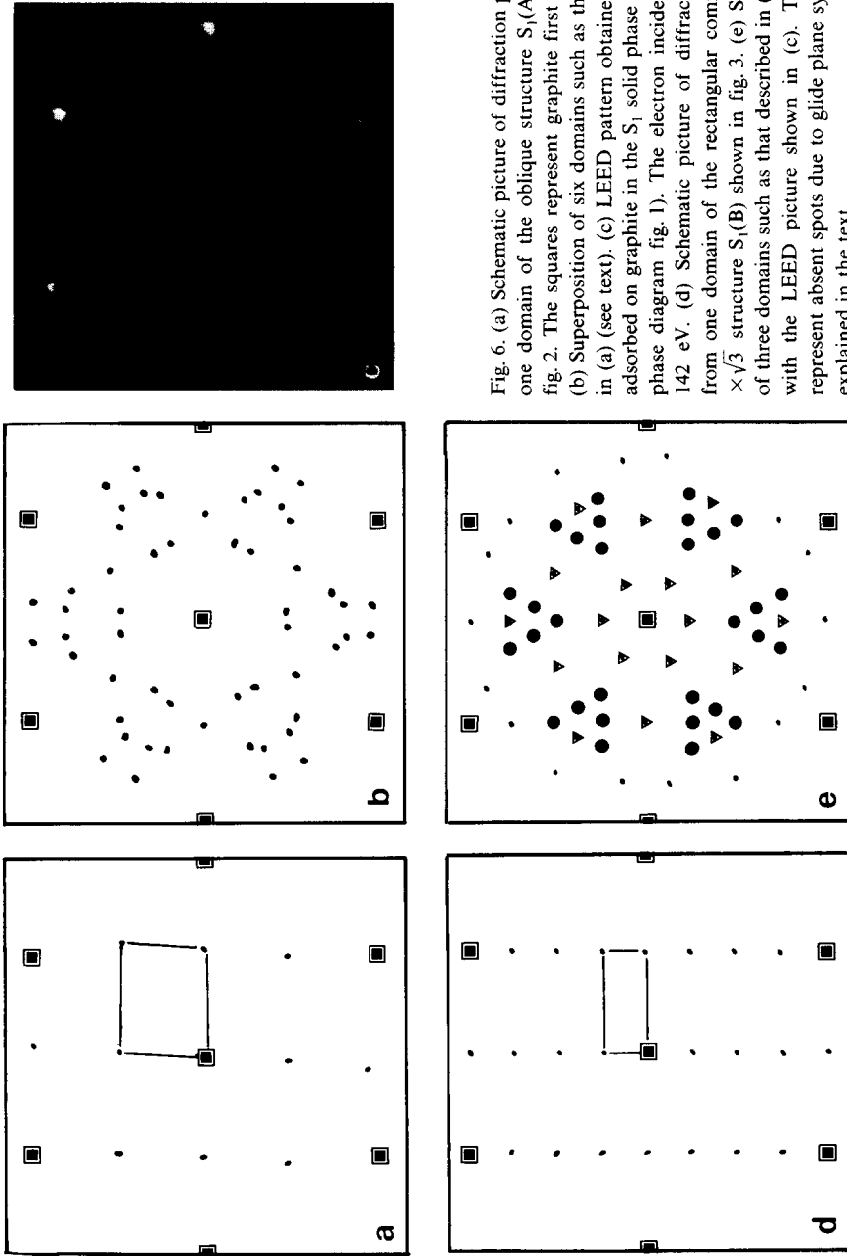
Fig. 6. (a) Schematic picture of diffraction pattern from one domain of the oblique structure $S_1(A)$ shown on fig. 2. The squares represent graphite first order spots. (b) Superposition of six domains such as that described in (a) (see text). (c) LEED pattern obtained for ethane adsorbed on graphite in the $S_1$ solid phase at 50 K (see phase diagram fig. 1). The electron incident energy is 142 eV. (d) Schematic picture of diffraction pattern from one domain of the rectangular commensurate $4 \times \sqrt{3}$ structure $S_1(B)$ shown in fig. 3. (e) Superposition of three domains such as that described in (d). It agrees with the LEED picture shown in (c). The triangles represent absent spots due to glide plane symmetries as explained in the text.
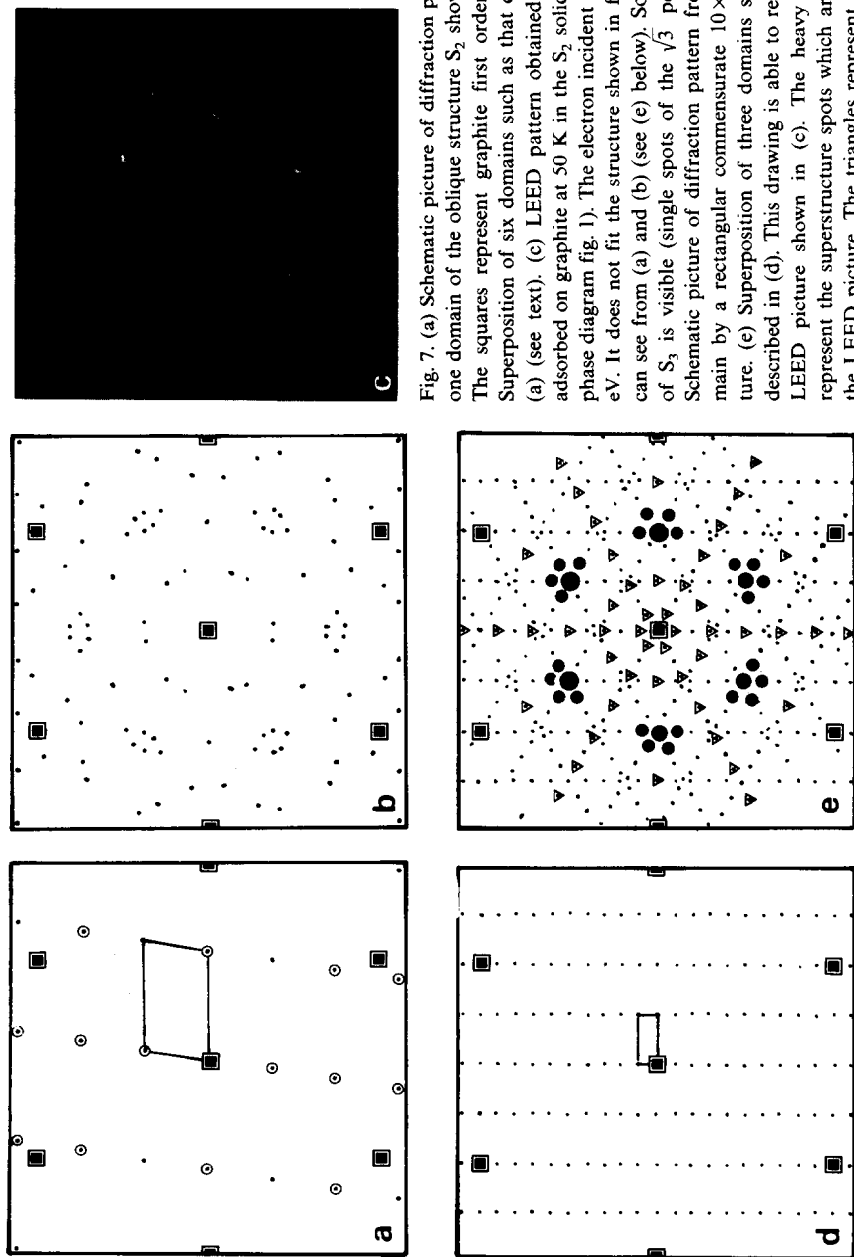
Fig. 7. (a) Schematic picture of diffraction pattern from one domain of the oblique structure S₂ shown in fig. 4. The squares represent graphite first order spots. (b) Superposition of six domains such as that described in (a) (see text). (c) LEED pattern obtained for ethane adsorbed on graphite at 50 K in the S₂ solid phase (see phase diagram fig. 1). The electron incident energy is 90 eV. It does not fit the structure shown in fig. 4 as one can see from (a) and (b) (see (e) below). Some amount of S₃ is visible (single spots of the √3 position). (d) Schematic picture of diffraction pattern from one domain by a rectangular commensurate $10 \times 2\sqrt{3}$ structure. (e) Superposition of three domains such as that described in (d). This drawing is able to reproduce the LEED picture shown in (c). The heavy full circles represent the superstructure spots which are visible on the LEED picture. The triangles represent spots which are missing possibly due to glide plane symmetries. The other dots are not visible in the LEED pattern (see text).

## 2.3. Solid $S_3$ (coverage 1.5)

With increasing coverage and $T \leq 55$ K, $S_2$ tranforms into $S_3$ through a first order phase transition. At coverage 1.5 pure $S_3$ is visible. The proposed structure is shown in fig. 5. It is a commensurate $\sqrt{3} \times \sqrt{3}$ cell with molecules standing on their methyl tripods above the graphite surface. The fact that $S_3$ exists alone only above the coverage 1.5 implies an appreciable amount of second layer. It is likely that this is necessary to stabilize the $S_3$ phase. It is not possible yet to tell whether $S_3$ is a solid bilayer or if the second layer is in a fluid-like state.

The melting of $S_3$ is quite different from $S_1$ or $S_2$. There appears to be no intermediate phase. $S_3$ melts between 82 and 87 K. We cannot yet tell the order of the transition. A remarkable result is that the coherence length of the liquid-like structure is still large at 87 K ($L \simeq 70$ Å) [18,20]. It is possible that $S_3$ behaves like xenon adsorbed on graphite above one monolayer coverage where the freezing transition is second order with very large fluid correlation lengths [32].

## 3. LEED experiments

The LEED system has been described elsewhere [33]. Let us recall that it has a four-grid optics with the fluorescent screen replaced by a channel plate–screen combination. It allows for a low current electron beam $I \simeq 10^{-9}$ A). Such a system has been used successfully in the study of physisorbed gases on graphite [11,15,33,34,38]. Besides the fact that the electron beam hardly perturbs the adsorbed phases, it allows the measurement of interatomic spacings with an accuracy of 1% or better. In the present study, it is remarkable that the electron beam does not crack the ethane molecule. Such a cracking has been observed with methane producing an irreversible contamination of the graphite surface [35].

A low temperature sample holder allows the graphite single crystal to be cooled down to 10 K [33] with a temperature regulation of $\pm 0.1$ K or better.

Before any experiment, ethane gas from Messer Griesheim, Dusseldorf (99.5% grade), is first introduced into a one litre gas tank at a pressure of about 100 Torr. Then, it is condensed in  glass cold finger at liquid nitrogen temperature where it solidifies. At this stage, the pressure above it is around $5 \times 10^{-3}$ Torr. The remaining gas is pumped out using a turbomolecular pump and the background pressure is $\simeq 10^{-8}$ Torr. Solid ethane is then warmed up and evaporated into the empty tank. This process is repeated 5 to 10 times until the equilibrium pressure above the solid ethane is that of pure ethane at 77 K, that is, $p \simeq 2 \times 10^{-4}$ Torr [36]. At this level of purification, no impurity is detectable in the gas phase.

The background pressure in the vacuum chamber being around $1 \times 10^{-10}$ Torr, we cool our graphite sample down to $T \simeq 50$ K. At this temperature, the equilibrium pressure of ethane condensed on graphite for coverages below one monolayer is several orders of magnitude below $10^{-10}$ Torr [37].

We introduce a pressure of $2 \times 10^{-9}$ Torr of ethane into the chamber and record the graphite (01) spot intensity versus time. The pressure is read on an ionization gauge and no thermomolecular correction is made. The low value of the pressure is chosen in order to allow thermal equilibrium between ethane molecules and the graphite surface to exist. We notice a linear decrease of the intensity due to ethane adsorption. After 20 min of exposure, a superstructure is observed on the LEED pattern. It is shown in fig. 6c. Ten minutes later, the intensity of the (01) graphite spot stabilizes and remains constant, then a new superstructure appears whose LEED pattern is shown in fig. 7c. Finally, after 40 min exposure at $2 \times 10^{-9}$ Torr of ethane, a new decrease in intensity is observed, followed by a plateau at constant intensity. After this last decrease, which is about 10% of that produced by the second structure, a third super-structure appears, as shown in fig. 8.

The experiment described above is quite reproducible and no contamination of the surface occurs due to cracking or gas impurities. As we will discuss in the next section, it is clear that the three successive solid phases observed in our LEED experiments are the $S_1$, $S_2$ and $S_3$ phases described in the preceding section.
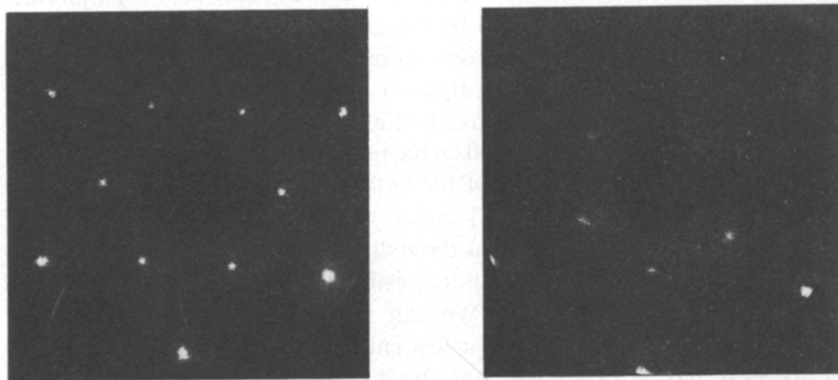


Fig. 8. LEED pattern obtained for ethane adsorbed on graphite at 50 K in the $S_3$ solid phase (see phase diagram fig. 1). The electron incident energy is 142 eV. $S_3$ is a $\sqrt{3} \times \sqrt{3}$ commensurate structure represented on figure 5 with a molecule separation equal to 4.26 Å.

Fig. 9. LEED pattern of ethane adsorbed on graphite at 63.5 K in the $I_1$ phase (see phase diagram fig. 1) close to the $S_1 \rightarrow I_1$ first order transition. One can see that the spots are broader than those of $S_1$ (fig. 6c) indicating rather short-range positional order. $I_1$ is a $2 \times 2$ commensurate phase with a molecule separation equal to 4.92 Å.

In these experiments, we also looked for the melting of $S_1$.

Once we get $S_1$ as indicated above, we decrease the ethane pressure to a few $10^{-10}$ Torr in order to maintain a constant coverage above the surface. Due to the very low equilibrium pressure, negligible desorption occurs and very little adsorption as well. Then we slowly increase the temperature unitl $S_1$ disappears and a new structure is observed at $T \simeq 63.5$ K. This new phase is shown in fig. 9. It has rather broad spots compared to $S_1$, $S_2$ or $S_3$. This new phase is certainly $I_1$ because the $S_1 \rightarrow I_1$ transition is observed around this temperature in the neutron experiments. Before closing this section, it is important to note that we have observed evidence of phase coexistence between $S_1$ and $S_2$, $S_2$ and $S_3$, $S_1$ and $I_1$, and the reversibility of the $S_1 \rightarrow I_1$ transition, all of which are in agreement with the neutron results. We have not yet investigated the $S_2 \rightarrow I_2$ transition.

## 4. Analysis of the LEED results

### 4.1. $S_1$ structure

The question is whether the $S_1(A)$ or $S_1(B)$ structures shown in figs. 2 and 3 can reproduce the LEED pattern shown in fig. 6c. In order to answer the question, we have drawn the reciprocal lattice of each structure at the same scale as the LEED picture. That of $S_1(A)$ is shown in fig. 6a and that of $S_1(B)$ in fig. 6d. For the oblique structure $S_1(A)$, there are six equivalent orientations in which the 2D lattice can be placed on the graphite surface at angles of 60° apart. There are three equivalent orientations for the rectangular structure $S_1(B)$. Hence, we have represented in figs. 6b and 6e the superposition of six domains like fig. 6a and three domains like fig. 6d respectively.

It is clear that there is a very good agreement between the LEED pattern and fig. 6e. The systematic absence of the $(h0)$ and $(0k)$ spots, with $h$ and $k$ odd numbers along the [10] and [01] directions (triangles in fig. 6e), are in agreement with the two glide planes in these directions, as discussed in section 2.1. Furthermore, the (04) and (0$\bar{4}$) spots, visible in the neutron experiments, are missing on the LEED pattern. We can explain this by the very weak scattering cross section of hydrogen for low energy electrons compared to that for neutrons. It has been shown that the LEED scattered intensity by a commensurate $\sqrt{3} \times \sqrt{3}$ monolayer of hydrogen molecules adsorbed on graphite is about $1/50$ that of graphite itself [38]. Hence, we calculated the diffracted intensities with ethane molecules in the $S_1(B)$ configuration, in the kinematical approximation, putting the atomic structure factor of hydrogen equal to zero. The result is quite convincing: the intensities of the missing spots are indeed negligible.

The spacings $d_{hk}$ measured from our LEED pattern are indicated in table 1

Table 1

Spacings $d_{hk}$ for the $S_1$ solid phase as determined from neutron diffraction and LEED experiments

| $d_{hk}$ (Å) | | | $hk$ |
|---|---|---|---|
| Theory | Neutrons [18–20] | LEED (present work) | |
| 4.92 | 4.93 | 4.88 ± 0.05 | (20) |
| 3.91 | 3.90 | 3.87 ± 0.04 | (11) |
| 3.22 | 3.21 | 3.21 ± 0.03 | (21) |
| 2.46 | 2.46 | – | (40) |
| 1.79 | 1.79 | – | (51) |
| 1.64 | 1.64 | – | (60) |

together with those determined from neutron experiments. The (51) and (60) spots are not visible on the LEED pattern because they are outside the screen.

To summarize, the preceding analysis shows that, for coverage below $\simeq 0.8$ monolayer and $T \leq 64$ K, the LEED pattern is consistent with the ethane molecules being arranged according to the $S_1(B)$ structure shown in fig. 3. It is a herring-bone structure with a rectangular centred unit cell and is commensurate $4 \times \sqrt{3}$ with the graphite substrate. Analysis of the LEED pattern does not give the orientation of the two molecules in the unit cell.

*4.2. $S_2$ structure*

As for $S_1$, we have drawn in fig. 7a the reciprocal lattice of the $S_2$ structure discussed in section 2.2. In fig. 7b, we have the superposition of six domains 60° apart as explained before. Comparing to our LEED observation shown in fig. 7c, it is easy to conclude that the structure proposed for $S_2$ does not explain the LEED pattern. Hence, the unit cell proposed in section 2.2, deduced from neutron diffraction experiments, is certainly not the correct one.

The only unit cell which can reproduce the LEED pattern and give the position of the numerous peaks observed in neutron diffraction experiments is shown in fig. 10. It is a $10 \times 2\sqrt{3}$ rectangular commensurate cell. The reciprocal lattice is shown in fig. 7d. Superposition of three domains 120° apart gives the pattern shown in fig. 7e. The triangles indicate extinguished spots if there were two glide planes as for $S_1(B)$. This is quite possible because the ($h0$) and ($0k$) spots ($k$ and $k$ odd) are not visible on the LEED pattern nor on the neutron spectra. Other spots are also missing but that could be due to structure factor effects. According to the coverage where $S_2$ appears alone, we estimate an approximate increase of 15 to 20% in the surface density when passing from $S_1$ to $S_2$. The areal density of $S_1(B)$ being 21 Å$^2$, that of $S_2$ should be around

17.5 Å². This implies 12 molecules per unit cell.

Because of the large number of molecules in the unit cell, it appears to be very difficult to undertake a structure factor analysis for $S_2$. However, the
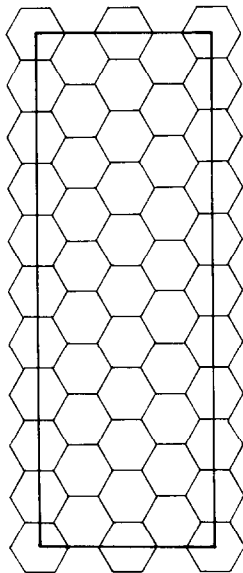


Fig. 10. Unit cell for the $10 \times 2\sqrt{3}$ $S_2$ structure. The number of molecules is probably 12 and their positions and orientations are not known yet. The position of the unit cell above the graphite surface is arbitrary.

possibile symmetries plus other extinctions may facilitate the calculations. Further simplification can be achieved by setting the structure factor of hydrogen equal to zero as we did for $S_1$ (see above).

We have given in table 2 the spacings $d_{hk}$ measured from the LEED pattern together with those determined from neutron experiments. We can notice that it is impossible to measure, within the experimental accuracy, any appreciable difference in the spacing $d$ for the (20) and (21) peaks both for neutron and LEED experiments. A larger number of Bragg reflections are observed in the neutron diffraction pattern. However, the great advantage of LEED is to separate clearly the symmetry-equivalent spots on the screen. Indeed, the fact that the unit cell $10 \times 2\sqrt{3}$ satisfies both the neutron and LEED results is very compelling. With a unit cell as large as $10 \times 2\sqrt{3}$, it would be quite difficult to solve the $S_2$ structure by either neutron diffraction or LEED alone.

To summarize, the unit cell proposed for $S_2$ from neutron diffraction experiments is not correct. However, by combining the large number of diffraction peaks in the neutron pattern with the symmetry of spots in the

Table 2
Spacings $d_{hk}$ for the $S_2$ solid phase as determined from neutron diffraction and LEED experiments

| $d_{hk}$ (Å) | | | $hk$ |
|---|---|---|---|
| Theory | Neutrons [18–20] | LEED (present work) | |
| 4.26 | | | (02) |
| | 4.28 | $4.24 \pm 0.04$ | |
| 4.20 | | | (12) |
| 3.69 | 3.68 | $3.71 \pm 0.04$ | (61) |
| 3.08 | | | (80) |
| | 3.01 | – | |
| 2.95 | | | (62) |
| 2.58 | 2.61 | – | (43) |
| 2.46 | | | (100) |
| | 2.46 | – | |
| 2.49 | | | (82) |

LEED pattern, it has been possible to deduce a $10 \times 2\sqrt{3}$ unit cell probably containing 12 molecules. This higher-order commensurate structure can explain the reason why there is no appreciable thermal expansion from 10 to 60 K as observed in the neutron experiments. However, the peak intensities begin to change at a lower temperature than in $S_1$ indicating [18–20] that $S_2$ is less stable than $S_1$. Possibly $S_2$ contains several distinct sites with different degrees of rotational order. The $S_2$ phase will be discussed further in the next section.

*4.3. $S_3$ structure*

We have nothing special to say about this phase. As shown on fig. 8, the LEED pattern indicates a $\sqrt{3} \times \sqrt{3}$ structure with a distance between molecules equal to 4.26 Å. This agrees with the neutron results described in the section 2.3.

*4.4. Melting of $S_1$*

From fig. 9 we see that at 63.5 K, $S_1$ has been transformed into a phase having a hexagonal symmetry. The value of the spacing $d$ measured on the LEED picture is $4.23 \pm 0.04$ Å. This is close to a $2 \times 2$ commensurate structure where the spacing $d$ is 4.26 Å which corresponds to a distance between molecules equal to 4.92 Å. The spots are broader than those of $S_1$ indicating a shorter range positional order.

These results are in agreement with the neutron experiments concerning the $S_1 \rightarrow I_1$ transition. Furthermore, they remove the uncertainty concerning the nature of $I_1$. It is certainly not the chain-like structure with positional disorder

within chains, because such an ordering would produce streaks in the LEED pattern.

We think that $I_1$ is an orientationally disordered triangular structure.
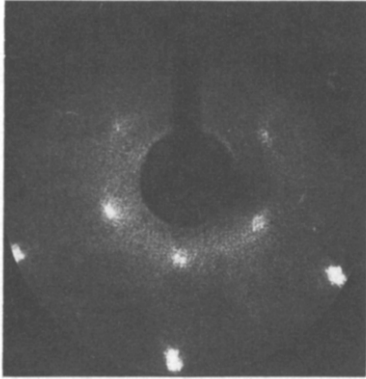


Fig. 11. LEED pattern of ethane adsorbed on graphite in the $I_1$ phase at 72 K. The spots are broader than those of fig. 9 at 63.5 K. $I_1$ transforms continuously into a liquid-like state.

Rotational motion has been observed in incoherent quasi-elastic neutron scattering experiments [39]. The small coherence length implies rather short range positional order. $I_1$ is probably formed of small commensurate $2 \times 2$ domains separated by walls of misfit dislocations. Let us notice that the $S_1$ 4 $\times \sqrt{3}$ solid and the $I_1$ $2 \times 2$ intermediate phase have exactly the same areal density equal to 21 Å$^2$.

When we increase the temperature, the $I_1$ spots become broader. Fig. 11 shows the LEED pattern at 72 K. If we further increase the temperature, we observe a broad ring-like pattern at $T \gtrsim 85$ K. We have not measured yet the mean distance between molecules in this liquid-like state from our LEED picture. However, the width of the ring pattern shows that there is a distribution of distances with possibly larger probability around the $2 \times 2$ spot, that is, 4.92 Å. This view is supported by the neutron results which show that the spacing $d$, as measured from the maximum of the (10) Bragg peak, does not change between 64 and 90 K. We did not observe abrupt changes in the LEED pattern between 64 and 85 K indicating that, to within the experimental resolution, a continuous transition takes place between $I_1$ and the liquid-like state.

## 5. Discussion and conclusion

It is clear that in the study of ethane adsorbed on graphite, our LEED experiments have given important new results on the nature of the various 2D phases.

This is the second example, after nitrogen, where an adsorbed rod like molecule likes to form a herring-bone structure at low temperature and submonolayer coverage. For nitrogen, this herring-bone structure was predicted theoretically using Lennard-Jones adsorbate–adsorbate and adsorbate–substrate interactions, plus quadrupole interactions between nitrogen molecules. In the case of ethane, very good agreement has been found between the observed herring-bone structure and that calculated from empirical potentials for the C–C, C–H and H–H pair interactions [18,20,40].

The sequence of first order transitions $S_1 \to S_2 \to S_3$ is very interesting. It has also been observed with another non-spherical molecule, nitric oxide, adsorbed on graphite [8,9]. One can ask the question: Is it a general phenomenon? In order to have a picture about what is happening when going from $S_1$ to $S_2$ and $S_3$, one can consider the Monte Carlo simulations made by O'Shea and Klein for classical quadrupoles on a triangular net [41]. When the substrate field is strong, molecules prefer to lie parallel to the substrate plane and a transition from orientational order to orientational disorder takes place at some critical temperature. If the substrate field is weak, then at low enough temperature the 2D phase is a mixture of molecules parallel and perpendicular to the surface. In the first case, at low enough temperature, the molecules arrange themselves into the herring-bone structure. In the second case (weak field), they give the so-called pin-wheel structure, which is very similar to the (111) plane of bulk $\alpha$-$N_2$(Pa3) structure.

Going from $S_1$ to $S_2$ is in some ways similar to changing the relative substrate field intensity. In the $S_2$ phase, lateral interactions may become predominant and some molecules may be tilted to give a structure similar to that described by O'Shea and Klein. Such a structure has a much larger unit cell than the herring-bone phase, although it is smaller than the $S_2$ unit cell. It is likely that in the case of ethane, the structure is more complicated. However, it is a starting point and it gives an attractive model to explain the $S_2 \to S_3$ transition where all molecules are probably perpendicular to the surface. Another interesting and striking behaviour of the three solids $S_1$, $S_2$ and $S_3$ is that the basis vector of one of the unit cells remains a multiple of $\sqrt{3}$. This may be due to an uniaxial compression of the layer along the [10] direction keeping the distance $\sqrt{3}$ between rows along the [01] direction.

As we pointed out in the introduction, the $S_1 \to I_1 \to L$ transitions raise questions of current interest concerning 2D melting and particularly that of 2D herring-bone structures. In the X-ray studies of the 650BC free standing liquid crystal films [23], the low temperature phase shows long range herring-bone order (smectic E). This phase transforms in a first order transition into a smectic B phase with short in plane positional order and long range, six-fold bond-orientational order. Then the smectic B phase transforms continuously into the smectic A with isotropic intralayer correlations.

This sequence of transitions is strikingly analogous to the $S_1 \to I_1 \to L$ transitions in ethane submonolayers.

Two-dimensional melting of anisotropic layers has been considered theoretically [42]. A sequence of transitions analogous to 650BC liquid crystal or ethane monolayers has been predicted. Of course, in the case of ethane films, the effect of the substrate field is to introduce a discrete set of preferred orientations. This affects the nature of the orientational order in the melted phase and instead of "quasi" long range orientational order in the absence of substrate, there is true long range orientational order.

It should be noticed that the way $S_1$ transforms into $I_1$ is slightly different from the orientational disordering transition of nitrogen [10,11]. Indeed, in the case of nitrogen, molecules remain attached at the centre of a graphite hexagon above the transition temperature. In the case of ethane, molecules are moving to settle into the $2 \times 2$ structure. However, as pointed out in section 4.4, $S_1$ and $I_1$ have exactly the same density as in the case of the two phases of nitrogen.

In summary, our LEED measurements have shown that the low coverage phase is a herring-bone structure at temperatures below 64 K which can be represented by a centred rectangular unit cell $4 \times \sqrt{3}$ commensurate with the graphite surface. As shown by profile analysis of the neutron diffraction pattern, this 2D solid $S_1$ has molecules with the C–C axes nearly parallel to the surface. The solid $S_1$ transforms at 64 K into an orientationally disordered phase $I_1$ which is $2 \times 2$ commensurate and has short-range positional order. This phase transition is first order. Then $I_1$ transforms apparently continuously into a liquid-like state. Hence, neutron and LEED data together give for the first time a complete solution of a 2D orientationally-ordered structure and describe its order–disorder transition towards melting.

Around coverage of one monolayer a new solid phase $S_2$ appears whose LEED pattern does not agree with the structure proposed in the neutron work. We deduced a $10 \times 2\sqrt{3}$ unit cell in order to reproduce the LEED pattern. The arrangement of molecules within the cell is not yet known.

Finally, above one monolayer appears a $\sqrt{3} \times \sqrt{3}$ solid phase with molecules probably having their C–C axes perpendicular to the graphite surface in agreement with the neutron results.

Further LEED experiments are being planned in order to study the critical exponent of the $I_1 \rightarrow L$ transition which is likely to belong to the four-states Potts model universality class [43,44]. We will also study the melting of $S_2$ and $S_3$.

## Acknowledgements

# References

[1] J.G. Dash, Films on Solid Surfaces (Academic Press, New York, 1975).

[2] M. Bienfait and J. Suzanne, Eds., Proc. Colloq. Intern. CNRS, Phases Bidimensionnelles Adsorbées, Marseille, France, 1977 [J. Physique C4 (1977)].

[3] J.G. Dash and J. Ruwalds, Eds., Proc. NATO ASI, Phase Transitions in Surface Films, Erice, Italy, 1979 (Plenum, New York, 1980).

[4] S.K. Sinha, Ed., Ordering in Two Dimensions (North-Holland, New York, 1980).

[5] P.I. Cohen, J. Unguris and M.B. Webb, Surface Sci. 58 (1976) 429.

[6] J. Unguris, L.W. Bruch, E.R. Moog and M.B. Webb, Surface Sci. 87 (1979) 415.

[7] J. Unguris, L.W. Bruch and M.B. Webb, Surface Sci. 114 (1982) 219.

[8] J. Suzanne, J.P. Coulomb, M. Bienfait, M. Matecki, A. Thomy, B. Croset and C. Marti, Phys. Rev. Letters 41 (1978) 760.

[9] J.P. Coulomb, J. Suzanne, M. Bienfait, M. Matecki, A. Thomy, B. Croset and C. Marti, J. Physique 41 (1980) 1155.

[10] J. Eckert, W.D. Ellenson, J.B. Hastings and L. Passell, Phys. Rev. Letters 43 (1979) 1329.

[11] R.D. Diehl, M.F, Toney and S.C. Fain, Jr., Phys. Rev. Letters 48 (1982) 177.

[12] G.J. Trott, H. Taub, F.Y. Hansen and H.R. Danner, Chem. Phys. Letters 78 (1981) 504.

[13] J.K. Kjems, L. Passell, H. Taub, J.G. Dash and A.D. Navaco, Phys. Rev. B13 (1976) 1446.

[14] Y. Larher, J. Chem. Phys. 68 (1978) 2257.

[15] R.D. Diehl, C.G. Shaw, S.C. Fain, Jr. and M.F. Toney, in ref. [4], p. 199.

[16] J.P. Coulomb, J.P. Biberian, J. Suzanne, A. Thomy, G.J. Trott, H. Taub, H.R. Danner and F.Y. Hansen, Phys. Rev. Letters 43 (1979) 1878.

[17] H. Taub, G.J. Trott, F.Y. Hansen, H.R. Danner, J.P. Coulomb, J.P. Biberian, J. Suzanne and A. Thomy, in ref. [4], p. 91.

[18] G.J. Trott, PhD Thesis, University of Missouri–Columbia (1981).

[19] J.P. Coulomb, Thesis, Faculté des Sciences de Luminy, Université Aix–Marseille II (1981).

[20] H. Taub, G.J. Trott, F.Y. Hansen, H.R. Danner, J.P. Coulomb, J.P. Biberian and J. Suzanne, to be published.

[21] J.P. Biberian, J.P. Coulomb, J. Suzanne, G.J. Trott, H. Taub, F.Y. Hansen and H.R. Danner, in: Proc. ICSS-4 and ECOSS-3, Cannes, 1980 [Le Vide, Les Couches Minces 201, Vol. I (1980) 126].

[22] J. Doucet, J. Physique Lettres 40 (1979) L185.

[23] R. Pindak, D.E. Moncton, S.C. Davey and J.W. Goodby, Phys. Rev. Letters 46 (1981) 1135. The 650BC is the n-hexyl-4'-n-pentyloxybiphenyl-4-carboxylate.

[24] R. Bruinsma and G. Aeppli, Phys. Rev. Letters 48 (1982) 1625.

[25] B.I. Halperin and D.R. Nelson, Phys. Rev. Letters 41 (1978) 121.

[26] D.R. Nelson and B.I. Halperin, Phys. Rev. B19 (1979) 2457.

[27] D. Frenkel and J.P. McTague, Phys. Rev. Letters 42 (1979) 1632.

[28] F.F. Abraham, Phys. Rev. Letters 44 (1980) 463.

[29] S. Toxvaerd, Phys. Rev. Letters 44 (1980) 1002.

[30] A.D. Novaco and P.A. Shea, to be published.

[31] International Tables for X-Ray Crystallography (Kynoch, Birmingham, 1965).

[32] P.A. Heiney, R.J. Birgeneau, G.S. Brown, P.M. Horn, D.E. Moncton and P.W. Stephens, Phys. Rev. Letters 48 (1982) 104.

[33] S. Calisti, J. Suzanne and J.A. Venables, Surface Sci. 116 (1982) 455.

[34] S.C. Fain, Jr., in: Proc. 5th Intern. Summer Institute in Surface Science, Milwaukee, WI, 1981 (Springer, Berlin, 1982).

[35] S.C. Fain, Jr., private communication.

[36] J. Régnier, J. Chim. Physique 69 (1972) 942.

[37] J. Régnier, Thesis, Université de Nancy (1976).

[38] J.L. Seguin and J. Suzanne, Surface Sci. 118 (1982) L241.

[39] J.P. Coulomb, M. Bienfait and P. Thorel, private communication.

[40] F.Y. Hansen, G.J. Trott and H. Taub, to be published.

[41] S.F. O'Shea and M.L. Klein, Chem. Phys. Letters 66 (1979) 381.

[42] S. Ostlund and B.I. Halperin, in ref. [4], p. 343.

[43] E. Domany, M. Schick, J. Walker and R.B. Griffiths, Phys. Rev. B18 (1978) 2209.

[44] J.S. Walker and M. Schick, Phys. Rev. B20 (1979) 2088.